Physics of Plasmas ARTICLE scitation.org/journal/php

A self-oscillating electron beam experiment

Cite as: Phys. Plasmas **27**, 023104 (2020); doi: 10.1063/1.5140037
Submitted: 25 November 2019 · Accepted: 13 January 2020 ·
Published Online: 4 February 2020

Meytal Siman-Tov,[a] John G. Leopold, and Yakov E. Krasik

AFFILIATIONS

Physics Department, Technion, Israel Institute of Technology, Haifa 3200003, Israel

[a]Author to whom correspondence should be addressed: meytalsh2@gmail.com

ABSTRACT

A recently proposed scheme to persistently over-inject a vacuum electron diode so that it self-oscillates, releasing a periodic train of electron bunches [Leopold *et al.*, Phys. Plasmas **24**, 073116 (2017)] was only partially demonstrated [Siman-Tov *et al.*, **26**, 033113 (2019)] because of the presence of hot spots on the dispenser cathode surface. The results obtained utilizing a new dispenser cathode with uniform surface emission, produce self-oscillations close to the expected frequencies.

I. INTRODUCTION

Space charge limited (SCL) emission and flow of electrons in vacuum are the foundations of charged particles beam dynamics since the 1D steady state Child-Langmuir law was formulated over a hundred years ago.[1] Vacuum electronics has been the basis of many applications some of which have been abandoned since solid state devices were developed, but many applications such as accelerators, x-ray guns, electron-microscopy, high power microwave devices, etc., require charged particle beams of different parameters.

Of particular interest is the instability which develops when a charge accumulates in a region above the space charge limit (SCL). The pioneering work of Birdsall and Bridges[2,3] predicted that if a vacuum gap is over-injected, that is, a beam carrying a current above the SCL is injected into this gap, a virtual-cathode (VC) forms which self-oscillates, so long as the injection persists. A VC is the collective response of charged particles in an over-charged space. The charged particles react to over-injection by slowing down completely at a downstream location along the flow from where for magnetized flow, they return toward the injection area to reduce the injected current. The potential distribution in a gap where the beam propagates changes when a VC appears. Assuming zero potential on the cathode and at the VC's downstream end, a negative potential well of depth equal or larger than the kinetic energy of the electrons is formed in between. The latter leads to a decreased effective gap between the VC downstream end and the anode and, consequently, to increased downstream current to the anode. The VC fills and drains of charge periodically and the flow becomes oscillatory, a property which has been utilized in vircators to produce high power microwaves[4] but a self-oscillating diode producing periodic electron bunches has not yet been demonstrated though ways to achieve this goal have been proposed.[5] Such high-frequency self-modulated electron beams can be used as electron sources for vacuum devices generating microwaves and intense high-frequency x-ray fluxes.

Recently, we have suggested a scheme in which an electron beam flows in a triode consisting of two gaps, accelerating in the first and decelerating in the second gap. Studies on electron oscillations in such a triode arrangement in a vacuum tube were first carried out in the pioneering work of Barkhausen and Kurz for microwave generation.[6] In our scheme, the decelerating voltage in the second gap determines whether this triode behaves like a vircator, when the second gap potential difference is zero ($\Delta V_2 = 0$), or a reflex triode, when the beam produced in gap 1 is fully decelerated in gap 2 ($0 < \Delta V_1 = -\Delta V_2$) (see Fig. 1: we refer to gaps 1 and 2, that is the region defined by the

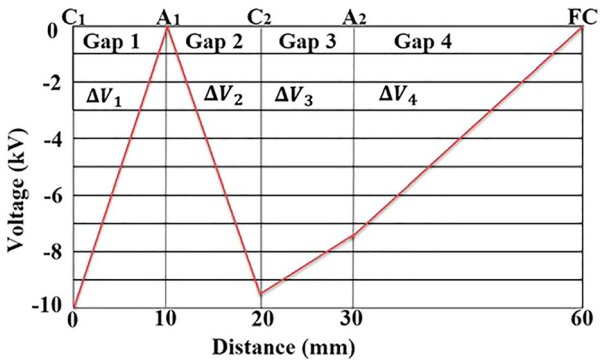

FIG. 1. The potential distribution in the tetrode. FC is a grounded Faraday cup used in the experiment to measure the collected beam.

electrodes C_1-A_1-C_2 as the *triode*).[7] We chose a slightly different situation, that is, a cathode emitting a current of amplitude below the SCL of the first gap and a potential difference in gap 2 which does not completely decelerate the beam so that there is no VC formation in this gap and the beam flows laminarly across the entire triode length. This stable beam is then injected into a consecutive third gap of a tetrode structure which we consider to be our diode (see Fig. 1: we refer to gap 3, C_2-A_2 as the *diode*, and C_1-A_1-C_2-A_2 as the *tetrode*). Whether the current flowing into the diode is below or above its SCL is determined by the voltage difference ΔV_3 in gap 3.[8] When it is above, it consists an over-injection, a VC forms near C_2 at the entry point of the injected beam to gap 3 from which currents flow both up and downstream. In Fig. 1, the electron emitting cathode is designated as C_1 and conducting transparent grids are located at the positions designated as A_1, C_2, and A_2. The overall flow from the cathode C_1 to the edge of the VC near C_2 can be considered as a flow in a *stretched* VC resulting in oscillations of frequency depending on the C_1–C_2 distance, i.e., the TOF of the oscillating electrons. We have demonstrated numerically[8] that downstream from C_2, the current flows in electron bunches when ΔV_3 is low enough and when ΔV_3 is increased, its flow becomes laminar.

We proceeded to demonstrate this model in an experiment which though seems very simple, was complicated by several obstacles.[9] We have shown that the value of ΔV_3 affected the flow, but we were unable to demonstrate current oscillations at the expected frequency. The explanation we offered was that our dispenser cathode's surface emitted electrons from random hot spots instead of being uniform [see Fig. 4 in Ref. 9 and Fig. 3(b) below]. In addition, the high voltage pulse applied to the dispenser cathode was not sufficiently constant in time and had a rise time of tens of ns. Simulations showed[9] that the effect of the rise time electrons on the dynamics is reflected in the presence of two modulation frequencies in the collected current. For a rise time of 20 ns, we calculated these to be 0.6 and 1.8 GHz. The single electron return transit time in an empty triode corresponds to a frequency of 0.8 GHz. The average plasma density in the VC near C_2 was $3 \times 10^{10}\,\mathrm{cm}^{-3}$ which corresponds to a plasma frequency of ~1.5 GHz. We concluded that the source for the low frequency current modulations is the electron motion along the VC stretched along the triode, whereas the higher frequency corresponds to the oscillations of the VC electron space charge. We also showed in Ref. 9 that the presence of the rise time electrons allows only current modulations rather than discrete electron bunches.

Here, we present new experimental results supported by MAGIC-PIC[10] simulations. We have been able to acquire a dispenser cathode which emits uniformly over its surface and we are now able to demonstrate the expected oscillatory behavior in the collected current.

II. EXPERIMENTAL SETUP

Our experimental setup is the same as that detailed in Ref. 9 and is seen in Fig. 2.

We replaced the dispenser cathode (Heatwave model 101439) with a new cathode developed by 3M-Ceradyne[11] in particular manufactured to avoid hot spots. The emission patterns of these two cathodes traced on a P43 Phosphor screen[9] placed at the same position as that of the low inductance Faraday cup in Fig. 2, are compared in Fig. 3. The uniformity of the 3M electron beam is clearly seen.

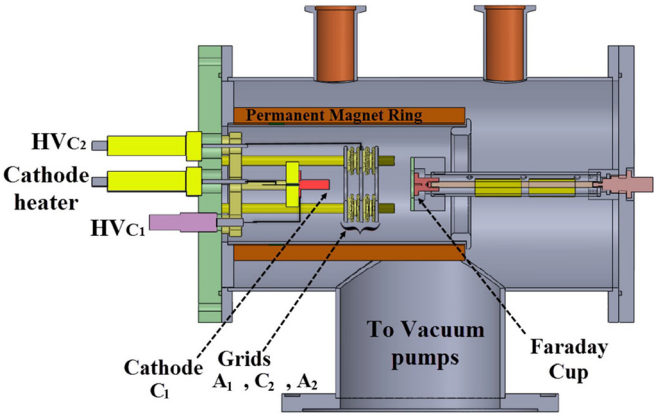

FIG. 2. Drawing of the experimental setup. (The thread connecting the A_2 grid to its high-voltage source is through the same flange as the other electrode connectors, but is not shown.) Reproduced with permission from Siman-Tov *et al.*, Phys. Plasmas **26**, 033113 (2019). Copyright 2019 AIP Publishing.

The cathode surface has a 6.35 mm diameter circular emitting area and when heated to 1200 °C, it emits a current of 1.26 A. The emitted beam is magnetized by an axial magnetic field of 540 G produced by permanent Neodymium magnet rings (N52) uniform in the relevant experimental volume. (Note that the value of the magnetic field in Ref. 9 was incorrectly quoted.) A pressure of 3×10^{-2} Pa is kept by scroll and turbo pumps. The grids A_1, C_2, and A_2 were 94% transparent 12 mm diameter Mo grids placed 10 mm apart. The transparency of these grids is of crucial importance because it determines losses of oscillating electrons. The distance of the A_1 grid from the cathode was also 10 mm and the FC (Faraday cup) was placed at a distance of 33 mm from the A_2 grid and was covered by a 54% transparent grid to decrease electromagnetic noise interference with the electron beam current waveform. The FC collector was connected to a 50 Ω coaxial cable RG 58.

A negative 10 kV, 850 ns long pulse with a rise time of 100 ns (Fig. 4) is supplied to the thermionic cathode (C_1) by a triggered pulse generator of four 10 nF capacitors connected in parallel and discharged through a fast high voltage transistor switch (Behlke, HTS 221-06). We replaced the Blumlein line based generator used in Ref. 9 with a solid-state generator based on a capacitor discharge by the Behlke high-voltage transistor switch in order to obtain a constant

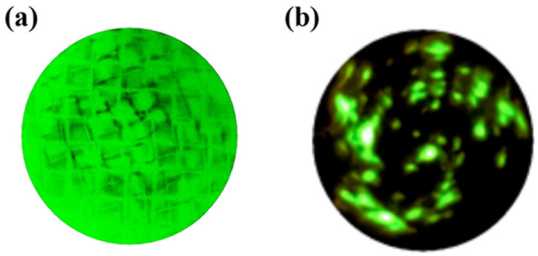

FIG. 3. The electron beam pattern emitted from (a) the 3M-Ceradyne cathode (1200 °C) and (b) the Heatwave cathode at 1270 °C as traced on the phosphor screen. The rectangular patterns seen in (a) reflect the presence of the grids. Panel (b) is reproduced with permission from Siman-Tov *et al.*, Phys. Plasmas **26**, 033113 (2019). Copyright 2019 AIP Publishing.

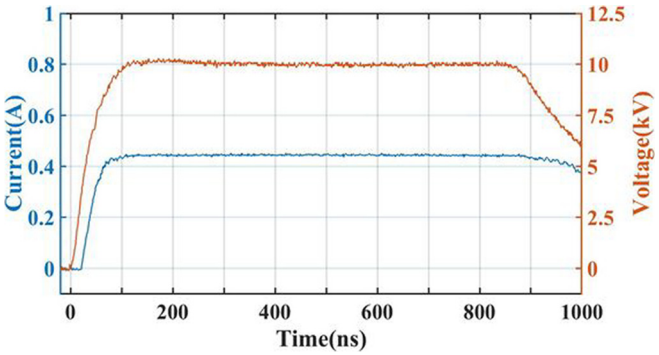

FIG. 4. The voltage pulse applied on the dispenser cathode and the current arriving to the FC for $\Delta V_2 = \Delta V_3 = \Delta V_4 = 0$.

amplitude plateau following the rise time and to be able to control the length of the pulse. To decouple the high voltage power supply from the dc power supply of the cathode heater, we used the same LC filter as described in Ref. 9. The A_1 and the FC grids are grounded whereas on C_2 and A_2, bias voltages are applied by discrete DC power supplies. To keep constant bias voltages, 2 nF capacitors were connected in parallel to C_2 and A_2. Using a calibrated P6015A Tektronix probe, we verified with an accuracy of ± 10 V that the absorption of a small part of the oscillating electrons by these finite transmission grids, does not change the bias voltage. The dc voltages on the grids C_2 and A_2 were measured by Fluke voltage dividers and the waveforms of the voltage pulse applied to the dispenser cathode and the cathode current were measured by a calibrated high-voltage P6015A Tektronix probe and a CT-1 Tektronix current transformer, respectively. Both the P6015A probe and the CT-1 current transformer were placed at the output of the high voltage pulse generator.

The voltage pulse applied on the dispenser cathode is seen in Fig. 4. The rise time of this pulse is ~100 ns and the 10 kV amplitude is constant for ~800 ns. For a voltage pulse of 10 kV amplitude, as shown in Fig. 4, the total emitted current, measured by the CT-1 probe, was 1.26 A. The collected current was measured on the FC with C_2 and A_2 grounded. The amplitude of the current collected on the FC was 0.44 A (see Fig. 4) which, corresponds to a beam current of 0.81 A arriving to the FC grid. The latter we define as the *collected* current.

In Fig. 5, we PIC simulate the experiment for the conditions shown in Fig. 4. The emitter of the dispenser cathode is 0.7 mm thick

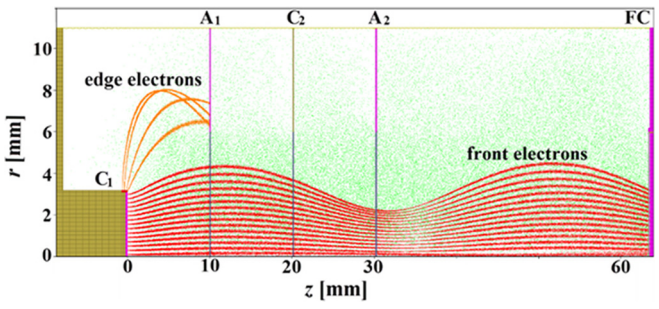

FIG. 5. Trajectories of electrons in the system for $\Delta V_1 = 10$ kV, $\Delta V_2 = \Delta V_3 = \Delta V_4 = 0$, and $B_z = 540$ G. The red dots are emitted electrons, whereas the green dots are secondary electrons resulting from grid collisions.

and has a 3.175 mm radius frontal circular surface. The diameter of the Mo grids is 12 mm and electrons emitted from the edge of the cathode do not cross the grids but impact the holder of grid A_1. The calculated total emitted current for an applied cathode voltage of 10 kV is 1.26 A the same as the measured value, divided between a frontal current of 0.83 A and a 0.43 A edge current. The current arriving to the FC after traveling through three 94% transparency grids and the 54% transparency FC grid was 0.4 A. Nonetheless, it is very possible that the corner of the emission surface is not well modeled compared to the experimental situation and that the simulations do not reflect the experiment exactly despite this agreement.

III. EXPERIMENTAL RESULTS AND PIC SIMULATIONS

In all our present experiments, the rise time of the voltage pulse is of the order of 100 ns. For a fixed decelerating voltage in gap 2, as the voltage increases during the rise time, low energy electrons are produced which oscillate between gaps 1 and 2 where charge accumulates and only when electrons reach sufficient energy, they cross into gap 3. We shall refer below to the low energy electrons produced during the rise time as *rise time electrons*. The rise time electrons affect the dynamics of the flow and the charge accumulated in the triode affects electron emission.[9]

In Fig. 6, we present the collected currents, for $\Delta V_1 = 10$ kV, $\Delta V_3 = -\Delta V_2$, and $\Delta V_4 = 0$ and different values of ΔV_2 in the decelerating gap 2, A_1–C_2.

For $\Delta V_2 = -9.2$ kV, the maximum amplitude of the collected current is close to that obtained for $\Delta V_2 = 0$, that is, the entire emitted current, apart from the edge current stopped in gap 1 and the current stopped by the grids, is transmitted almost unperturbed. Note that no current is observed for more than ~100 ns compared to Fig. 4, where electrons are not slowed down in gap 2 ($\Delta V_2 = 0$) and there is only a short (a few ns) delay between the voltage and the collected current which corresponds to the transit time of the 10 keV electrons from the cathode to the FC. As $|\Delta V_2|$ increases, electrons flowing downstream from the triode gain lesser initial energy and more space charge accumulates in the triode releasing less current downstream (Fig. 6). For $\Delta V_2 = -9.4$ kV, the current amplitude rises to the maximum value

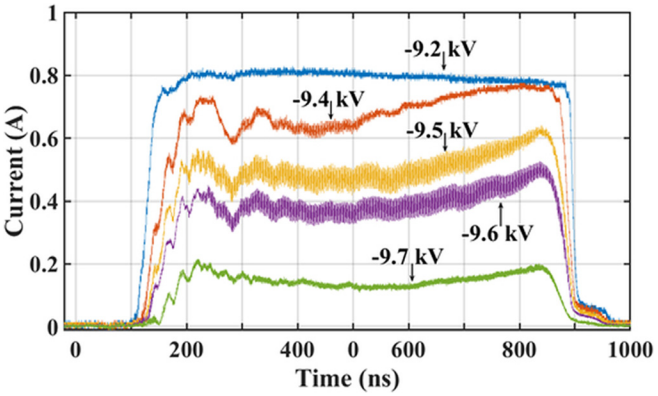

FIG. 6. Experimental results showing the collected current measured for different values of ΔV_2, and $\Delta V_1 = 10$ kV, $\Delta V_3 = -\Delta V_2$, and $\Delta V_4 = 0$. (The different values of ΔV_2 are pointed out in the figure.) Here, zero time is the time when the high voltage pulse is applied to the cathode C_1.

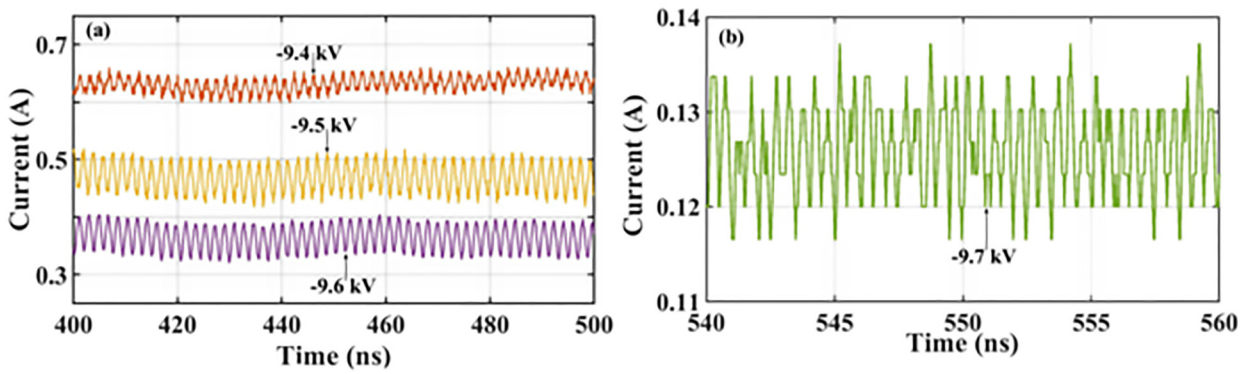

FIG. 7. A magnified region of Fig. 5 for $\Delta V_2 = -9.4$, -9.5, and -9.6 kV (a) and -9.7 kV (b).

only after ~750 ns. This tendency is seen for the other values of ΔV_2 drawn in Fig. 6 but none reach the maximum current during the experimental pulse length.

In the experiments presented in Ref. 9, we assumed that the reason we did not observe the predicted oscillations was due to the nonuniform cathode emission (see Fig. 3). Here, in Fig. 6, for $\Delta V_2 = -9.5$ and -9.6 kV, we observe clear oscillations at a frequency of 0.54 GHz as seen in the magnified curves in Fig. 7(a). Small amplitude oscillations at the same frequency exist even for -9.4 kV which disappear as the current increases.

The measured frequency of 0.54 GHz seen in Fig. 7(a) is of the same order as the estimated frequency of a single electron return transit time in the triode (0.8 GHz), neglecting the presence of space charge. Therefore, we think that the observed current oscillations reflect the oscillatory behavior of the electrons in the triode as suggested in Ref. 9. For $\Delta V_2 = -9.7$ kV, the amplitude of the collected current in Fig. 6 is very small though it is possible to discern ~2 GHz oscillations for this value when magnified in Fig. 7(b).

Oscillations at 0.54 GHz frequency are also observed by measuring the emitted current using the CT-1 current transformer. For example, for $\Delta V_2 = -9.5$ kV and $\Delta V_3 = -\Delta V_2$, $\Delta V_1 = 10$ kV, and $\Delta V_4 = 0$, the oscillatory behavior of the emitted current in the interval 600–650 ns is seen in Fig. 8. This proves that the charge oscillating in the triode affects the emission as predicted.[9] The CT-1 transformer foil has a bandwidth of 1 GHz and therefore it cannot resolve 2 GHz frequency.

In Fig. 9, we present the experimental results for the conditions $\Delta V_1 = 10$ kV, $\Delta V_2 = -9.5$ kV, and -9.7 kV, while the accelerating voltage ΔV_3 in the gap 3 is varied. For these values of ΔV_2, the initial energy of the electrons entering gap 3 is at most 500 eV and 300 eV, respectively. One can see that as ΔV_3 is reduced, the current crossing into gap 3 decreases. A finite low current is observed even when $\Delta V_3 = 0$. In order to increase the effect of over-injection of the diode of gap 3, it would have been advantageous to reduce the initial energy (increase ΔV_2) even more than in Fig. 9(b), but this is not possible in these experiments because the current is too low to detect accurately.

There are very long period amplitude variations during the current rise time in Fig. 9 which we think are the results of the interference of the charge cloud accumulated in the triode with the dispenser cathode's emitting surface. When the accumulated oscillating charge nears the emitter, it causes it to reduce the emitted current. Such behavior may cause the experimental cathode to behave irregularly during the rise time. Indeed, we found that the cathode had a much shorter lifetime than that claimed by the manufacturer and it is possible that the back-bombardment of the emission surface was the cause for this. Other than this, regular oscillatory behavior can be discerned for both cases in Fig. 9. The frequency of these oscillations is 0.54 GHz for all cases in Fig. 9(a) and oscillations can be discerned even for $\Delta V_2 = -9.5$ kV and $\Delta V_3 = 0$. For $\Delta V_2 = -9.7$ kV, the frequency of the oscillations for all cases with discernible oscillations is 2 GHz [Fig. 9(b)]. In Fig. 10, we magnify the oscillatory behavior for two cases chosen from Fig. 9 to display the oscillatory behavior more clearly.

The dynamics of such experiments was analyzed in Ref. 9 by PIC simulations. Since the experimental conditions are now different, we performed a few additional simulations to explain our experimental results. In the simulations, the electrons are emitted using the MAGIC-PIC code's thermionic emission model, but we chose a shorter rise time (20 ns) than in the experiments because of computer power limitations.

In Fig. 11, the PIC simulated time dependence of the collected current for $\Delta V_2 = -9.5$ kV and $\Delta V_3 = 6$ kV is shown. The simulated collected current displays ~0.8 GHz oscillations in the ~20–50 ns region, which settle at a fixed value higher than in the experiment [Fig.

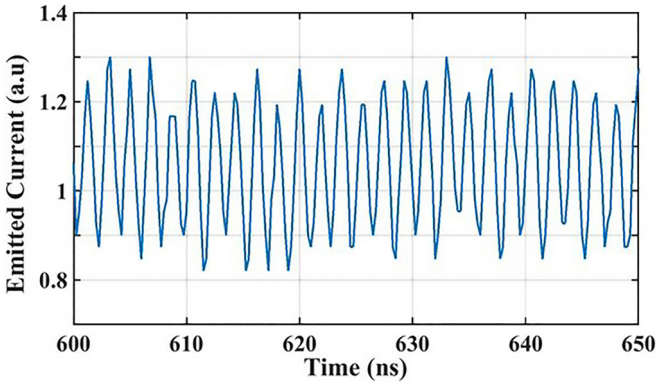

FIG. 8. The measured emitted current in the enlarged time interval 600–650 ns for $\Delta V_2 = -9.5$ kV, $\Delta V_3 = -\Delta V_2$, $\Delta V_1 = 10$ kV, and $\Delta V_4 = 0$.

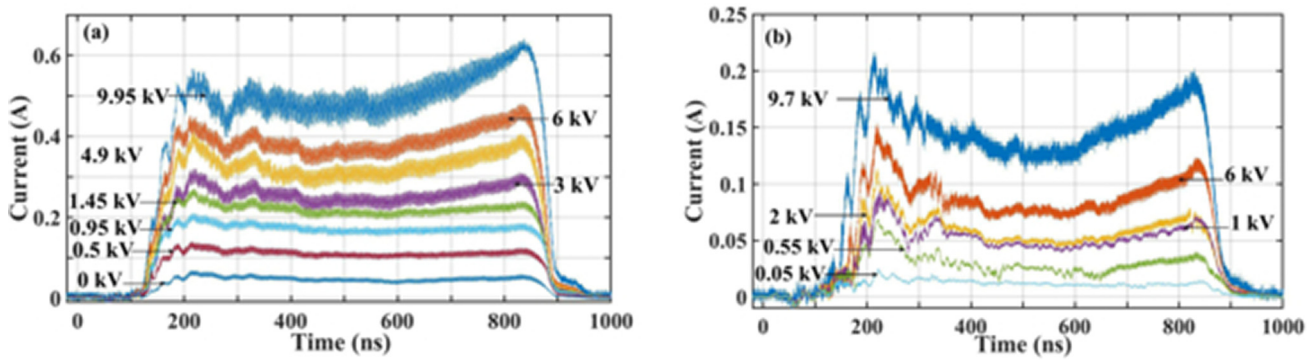

FIG. 9. Experimental results showing the collected current measured for different values of $\Delta V_1 = 10$ kV, $\Delta V_4 = 0$ and decelerating voltage in gap 2, $\Delta V_2 = -9.5$ kV (a) and -9.7 kV (b) (different values of the accelerating voltage in gap 3, ΔV_3, are pointed out in the figure).

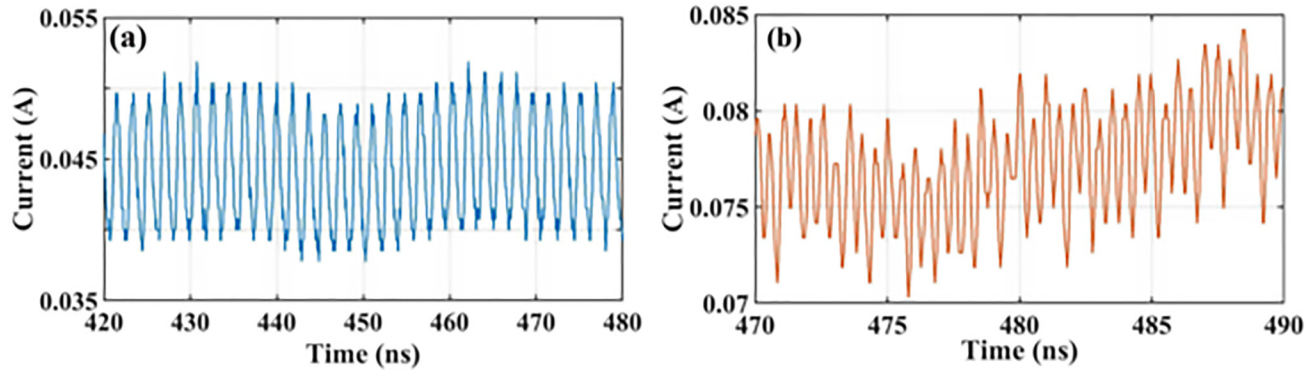

FIG. 10. A magnified region of the experimental signals in Fig. 9 for (a) $\Delta V_2 = -9.5$ kV, $\Delta V_3 = 0$ and (b) $\Delta V_2 = -9.7$ kV, $\Delta V_3 = 6$ kV, and $\Delta V_1 = 10$ kV.

9(a)]. In Fig. 9(a), the frequency of the oscillations, when present, is 0.54 GHz for all values of ΔV_3.

In Fig. 12, the (z, p_z) phase-space and charge density contours at various times in Fig. 11 are displayed. The rise time electrons (blue) are distinguished from the post rise time ones (red) [Figs. 12(a), 12(c) and 12(e)]. During the rise time, the energy of the electrons increases which is the cause for the rise time electrons to be smeared inside the phase-space-island (blue dots in Figs. 12(a)–12(c)). The island itself shifts so that its edges ($p_z \sim 0$) move during a period of an oscillation of the collected current (0.8 GHz), from C_1 to C_2 and back [see Fig. 12(a) and about half a period later in Fig. 12(c)]. When the rise time electron island edge is close to C_1, it forms large space charge near the cathode [Fig. 12(b)] which reduces the emitted current. At the same time, a high charge density forms near C_2 in the C_2-A_2 gap [Figs. 12(b) and 12(d)] made up of high energy post rise time electrons [Fig. 12(a)]. When the rise time island moves away from the cathode and closer to C_2 [Fig. 12(c)], the space charge near C_1 decreases and the space charge in gap C_2-A_2 moves into gap A_1-C_2. These oscillations of the rise time phase-space island between C_1 and C_2 are responsible for the oscillations seen in Fig. 11. At longer times, the oscillations in Fig. 11 stop, the rise time electrons drain out [Fig. 12(e)], and the post-rise time electrons flow unperturbed from the fixed charge density area near C_2 [Fig. 12(f)].

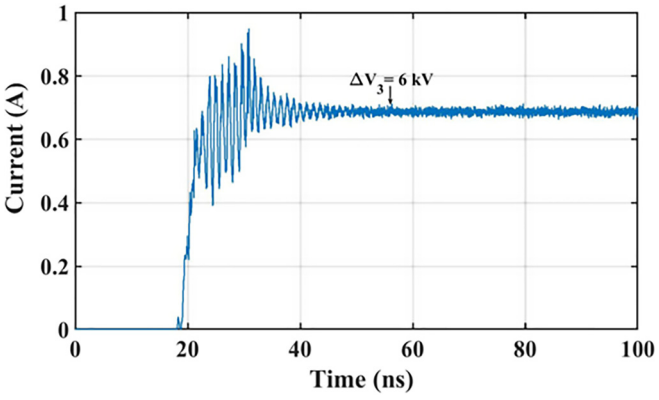

FIG. 11. PIC simulated time dependence of the collected current for $\Delta V_2 = -9.5$ kV and $\Delta V_3 = 6$ kV, and $\Delta V_1 = 10$ kV.

In the experiments, the oscillations persist for a very long time because the rise time of the applied voltage pulse is much longer and the rise time electrons do not drain out during the entire pulse.

It is difficult to reconstruct the experimental results for the same voltages because of the relatively small rise time considered in the simulations. In Fig. 13, the MAGIC-PIC simulated time dependence of the collected current for $\Delta V_2 = -9.9$ kV and $\Delta V_3 = 9.9$ kV is shown. For these conditions, oscillations of 1.8 GHz frequency are observed

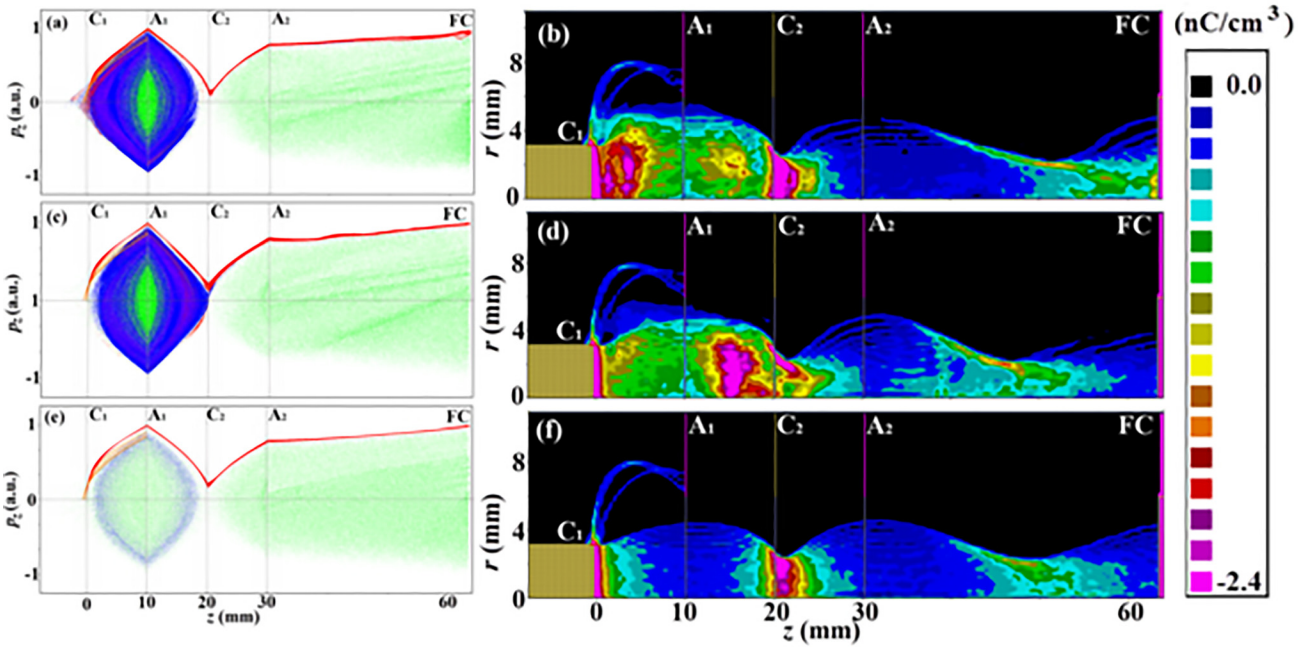

FIG. 12. PIC simulated (z, p_z) phase space (left panel) and contours of charge density (right panel) for $\Delta V_1 = 10$ kV, $\Delta V_2 = -9.5$ kV, $\Delta V_3 = 6$ kV, and $t = 27.086$ ns (a) and (b), 27.685 ns (c) and (d), and 63.216 ns (e) and (f). The colors in the left panel distinguish between: rise time electrons (blue), post-rise time electrons emitted at $t \geq 20$ ns (red), and electrons scattered from the grids (green).

along the entire simulation time. We have chosen a higher value of $|\Delta V_2|$ instead of that in the experiment [Fig. 9(b)] because in the simulations, the frequency change does not occur for lower values. Also, note that the collected current amplitude is higher than in the experiment. This is probably because of the much longer experimental rise time of the applied voltage, which retains the low energy rise time electrons for much longer.

In Fig. 14, we draw the same type of simulation results as in Fig. 12 for the conditions of Fig. 13. Here, in contrast to Fig. 12, the post rise time emitted electrons also oscillate in the triode phase-space island because they are much more slowed down and can return upstream [Figs. 14(a), 14(c), and 14(e)]. Simulations show that

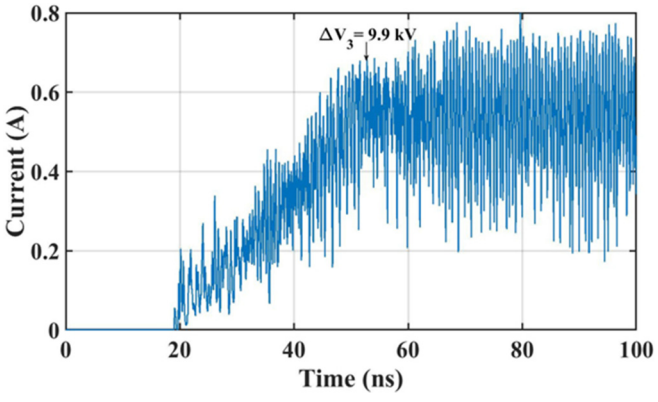

FIG. 13. PIC simulated time dependence of the collected current for $\Delta V_1 = 10$ kV, $\Delta V_2 = -9.9$ kV, and $\Delta V_3 = 9.9$ kV.

electrons start to deplete from the triode already at $t \sim 18$ ns when the collected current starts to increase. By $t \sim 50$ ns, the rise time electrons are fully depleted and the post rise time electrons continue to oscillate in the triode. In the triode, there are regions with an average electron density of 5×10^{10} cm^{-3} located near C_1 and C_2 [Figs. 14(b), 14(d), and 14(f)] which oscillate locally. Note the difference in phasespace near C_2 between Fig. 14(c) and about half a period later in Fig. 14(c). This electron density corresponds to a plasma frequency of 1.8 GHz in agreement with the experimental oscillation frequency 2 GHz of the collected current. Thus, for this case, the presence of the rise time electrons has little effect but the oscillating frequency is not connected to the TOF of electrons in the triode.

IV. CONCLUSIONS

In Ref. 9, we have shown that rise time electrons have a crucial effect on the dynamics of this system and that these electrons allow current modulations but avoid the formation of discrete electron bunches. Nonetheless, we predicted two types of current oscillations to develop. Low frequency current oscillations, the result of electron transit time movement in the triode and high frequency plasma density oscillations. In Ref. 9, we were unable to observe this and we assumed that the reason for this was that the emitting surface of the dispenser cathode emitted from hot spots rather than from the entire surface. The dispenser cathode used in the present research was different in this sense and emitted uniformly from its entire surface (Fig. 3).

With this cathode we demonstrated, depending on the experimental conditions, the oscillatory behavior of the collected current at 0.54 and 2 GHz which should be compared to the PIC simulated values of 0.8 and 1.8 GHz, respectively. We think that the differences between the simulations and the experiment are the result of the

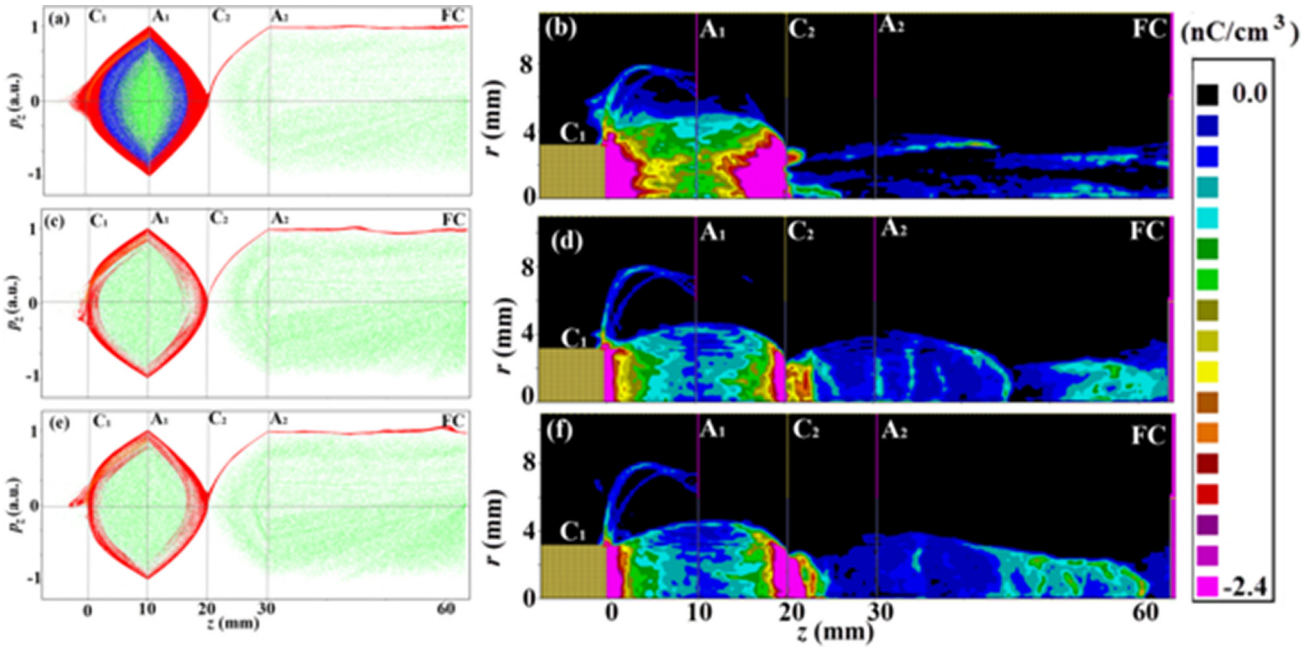

FIG. 14. Same as Fig. 12 for $\Delta V_1 = 10$ kV, $\Delta V_2 = -9.9$ kV, and $\Delta V_3 = 9.9$ kV for $t = 40.573$ ns in (a) and (b), 85.205 ns in (c) and (d), and 85.454 ns in (e) and (f).

longer experimental voltage rise time compared to that used in the simulations and that we are uncertain if the edge of the emitting surface is simulated correctly.

The thermionic cathode seems not to have been the best choice for demonstrating our model presented in Ref. 8 to produce over-injection, resulting in a train of electron bunches. It was, though, a sensible choice because the model required the use of a cathode operating below its space charge limit. The main drawbacks of the thermionic electron source are the necessity of high vacuum (better than 10^{-5} Pa) and degradation of its surface emission uniformity because of back-bombardment of ions from background gas ionization and sputtering of the grids by the electron beam interaction. We now pursue our goal to produce trains of electron bunches from self-oscillating devices by using high voltage cathodes emitting electrons at their space-charge limit using a different scheme.[12]

ACKNOWLEDGMENTS

The authors are grateful to Svetlana Gleizer, Irena Feldman, and Eugene Flyat for their invaluable technical assistance.

REFERENCES

[1]P. Zhang, A. Valfells, L. K. Ang, J. W. Luginsland, and Y. Y. Lau, Appl. Phys. Rev. **4**, 011304 (2017).
[2]C. K. Birdsall and W. B. Bridges, J. Appl. Phys. **32**, 2611 (1961).
[3]W. B. Bridges and C. K. Birdsall, J. Appl. Phys. **34**, 2946 (1963).
[4]J. Benford, J. A. Swegle, and E. Schamiloglu, *High Power Microwave* (Taylor & Francis Group, 2007).
[5]A. Pedersen, A. Manolescu, and Å. Valfells, Phys. Rev. Lett. **104**, 175002 (2010).
[6]H. Barkhausen and K. Kurz, Phys. Ztg. **21**, 1 (1920) (in German).
[7]Y. A. Kalinin, A. A. Koronovskii, A. E. Khramov, E. N. Egorov, and R. A. Filatov, Plasma Phys. Rep. **31**, 938 (2005).
[8]J. G. Leopold, M. Siman-Tov, A. Goldman, and Y. E. Krasik, Phys. Plasmas **24**, 073116 (2017).
[9]M. Siman-Tov, J. G. Leopold, and Y. E. Krasik, Phys. Plasmas **26**, 033113 (2019).
[10]B. Goplen, L. Ludeking, D. Smith, and D. Warren, Comput. Phys. Commun. **87**, 54 (1995).
[11]R. L. Ives, L. R. Falce, S. Schwartzkopf, and R. Witherspoon, IEEE Trans. Electron Dev. **52**, 2800 (2005).
[12]J. G. Leopold, Y. P. Bliokh, M. Siman-Tov, and Y. E. Krasik, Phys. Plasmas **26**, 093107 (2019).